Special Section: Dissolved Organic Matter in Soil

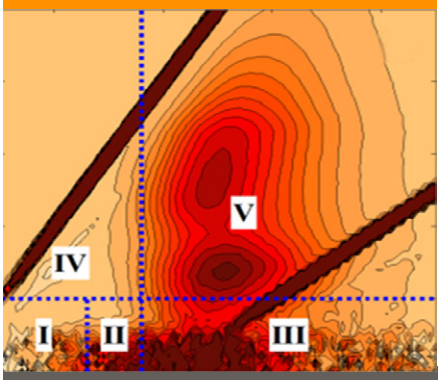

Natural organic matter is subjected to kinetic exchange on Al and Fe oxy(hydroxide) coated sand surfaces during laboratory experiments.

Fractionation of Dissolved Organic Matter by (Oxy)Hydroxide-Coated Sands: Competitive Sorbate Displacement during Reactive Transport

Angélica Vázquez-Ortega, Selene Hernandez-Ruiz, Mary Kay Amistadi, Craig Rasmussen, and Jon Chorover*

Sorptive retention of dissolved organic matter (DOM) at soil particle surfaces controls C flux through the critical zone. Prior studies have shown that pristine Al- and Fe-(oxy)hydroxide surfaces are especially reactive toward DOM sorptive stabilization. However, the impact of progressive and/or preexisting organic surface coatings on further surficial uptake and exchange during repeated DOM infusion episodes remains unclear. In this study, DOM solutions were extracted from organic horizons in grassland (G) and mixed conifer forest (F) vegetation types in the Jemez River Basin Critical Zone Observatory. Extracted DOM solutions were used to sequentially irrigate columns packed with either quartz sand (Qtz), Al-hydroxide-coated quartz sand (Al-Qtz), or Fe-hydroxide-coated quartz sand (Fe-Qtz). Use of distinct DOM sources enabled investigation of how sorption, fractionation, and exchange ensued during reactive transport through mineral media progressively coated with sorbate organic matter (SOM). During initial irrigation of fresh mineral media with G-DOM, the magnitude of DOM sorption (per unit sorbent mass) followed the trend: Al-Qtz $\geq$ Fe-Qtz > Qtz. Effluent solutions showed diminished molar absorptivity and humification index (HIX) values, indicating preferential uptake of high-molar-mass aromatic constituents. Introduction of F-DOM to G-SOM-coated surfaces revealed competitive desorption of G-SOM from the organo–mineral interface. During F-DOM irrigation, high HIX values were observed in effluent solutions, indicating remobilization of G-SOM by displacement. According to spectroscopic analyses, the displaced G-SOM consisted of aromatic phenolic acids with high excitation–emission "fingerprints" characteristic of fulvic- and humic-acid-like compounds, providing evidence for kinetic DOM exchange reactions.

Abbreviations: Al-Qtz, aluminum-hydroxide-coated quartz sand; DOC, dissolved organic carbon; DOM, dissolved organic matter; EEM, excitation–emission matrix; Em, emission; Ex, excitation; F, mixed conifer forest; Fe-Qtz, iron-hydroxide-coated quartz sand; FRI, fluorescence regional integration; G, grassland; HIX, humification index; OM, organic matter; PV, pore volume; Qtz, quartz sand; SOM, sorbate organic matter; UV-Vis, ultraviolet–visible wavelengths.

The elucidation of biogeochemical mechanisms that stabilize and destabilize C in soils is important to understanding C cycle feedbacks to climate change (Six et al., 2002; Goh, 2004; von Lützow et al., 2006, 2008; Hedman et al., 2013a, 2013b). Among the various processes involved in dissolved organic matter (DOM) stabilization, adsorption at Al- and Fe-(oxy)hydroxide surfaces is important (Eusterhues et al., 2003, 2005; Kaiser and Guggenberger, 2000; Chorover and Amistadi, 2001; Chi and Amy, 2004; Gu et al., 1994, 1995; Guo and Chorover, 2003, 2006; Hunt et al., 2007; Meier et al., 1999; Namjesnik-Dejanovic et al., 2000; Zhou et al., 2001; Kaiser et al., 1997, 2007). Although Al and Fe oxides often represent a small total mass fraction of the soil mineral mass, they exert a disproportionate effect on interfacial reactions because of their nucleation and

Dep. of Soil, Water & Environmental Science, Univ. of Arizona, P.O. Box 210038, Tucson, AZ 85721-0038. *Corresponding author (chorover@cals.arizona.edu).

Vadose Zone J.
doi:10.2136/vzj2013.10.0179
Received 9 Oct. 2013.
Supplemental material online.

lateral growth on the surfaces of other minerals, including less DOM-reactive tectosilicates such as feldspars and quartz (Coston et al., 1995; Joo et al., 2008). However, the specific processes controlling organic matter (OM) complexation with oxide-coated surfaces and the mechanisms affecting exchange between DOM and sorbate organic matter (SOM) in the solid phase are not fully resolved. The proposed mechanisms controlling DOM sorption–desorption include anion exchange, ligand exchange–surface complexation, cation bridging, H bonding, van der Waals forces, and the hydrophobic effect (Eusterhues et al., 2005; von Lützow et al., 2006, 2008; Scheel et al., 2007; Joo et al., 2008).

Based on the polydispersity and polyfunctionality of DOM molecular species and the associated range of intermolecular associations with soil constituents (Mortland, 1970; Greenland, 1971; Theng, 1979; Sutton and Sposito, 2005; Lam and Simpson, 2008; Lattao et al., 2008; Simpson et al., 2012), Kleber et al. (2007) proposed a multifaceted "zonal" model of OM sorption at mineral–water interfaces, similar to that proposed earlier by Wershaw (1993). The zonal model assumes a DOM molecular structure consisting of small and chemically diverse organic molecules interlinked by hydrophobic, cation-bridging, and H-bonding interactions that are capable of self-organizing (pseudo-micellar) behavior in aqueous solution (Sutton and Sposito, 2005) and—by extension—at the mineral–water interface (Wershaw, 1993; Kleber et al., 2007). The model postulates the distribution of sorbed DOM among the (i) mineral contact zone, (ii) intermediate hydrophobic zone, and (iii) peripheral kinetic zone. If kinetically labile domains do indeed exist at the particle–OM interface, they should be measurable in DOM reactive transport experiments that use methods of detection that are sensitive to DOM molecular structure (e.g., ultraviolet–visible wavelengths [UV-Vis] and fluorescence excitation–emission spectroscopy) (Hunt and Ohno, 2007; Ohno et al., 2007, 2008; Hernandez-Ruiz et al., 2012).

Organic matter exchange reactions at mineral–water interfaces may be prevalent in terrain affected by shifts in hydrologic flow paths, and this probably affects the molecular composition of terrestrial DOM that is effluent to surface waters. For example, in catchments comprising grassland stands adjacent to mixed conifer forest on hillslopes (as occurs in mountain environments throughout the western United States), such intermixing and exchange reactions are likely to occur, for example, during near-surface runoff and subsurface flow, when the catchment subsurface is "connected" hydrologically (Perdrial et al., 2014). To the extent that DOM derived from distinct vegetation types differs in molecular composition (Sanderman et al., 2008), competitive adsorption–desorption reactions are likely to ensue.

Sensitive, nondestructive techniques, such as UV-Vis and fluorescence spectroscopy, can be used to obtain information about the DOM molecular structure (Her et al., 2003; Hunt and Ohno, 2007; Ohno et al., 2007, 2008; Hernandez-Ruiz et al., 2012). Fluorescence excitation–emission matrices (EEMs), in particular, contain information on spectrally distinct DOM components (Banaitis et al., 2006) and are highly sensitive to DOM structure and sorptive fractionation reactions (Hunt and Ohno, 2007; Hunt et al., 2007). Dissolved organic matter can be fingerprinted by its distinctive fluorescence properties (Baker et al., 2008; Bieroza et al., 2010; Her et al., 2003). Different regions of the EEM correspond to distinct organic moieties. For example, the protein-like region of the DOM EEM is represented by tryptophan and tyrosine compounds and includes methyl, methylene, hydroxyl, and amide functional groups (Clapp et al., 2001; Huo et al., 2008). The fulvic- and humic-like regions are more aromatic and hydrophobic in character, containing partially degraded lignin phenyl-propanoids, O-alkyl, carboxylic acids, amides, and thiols, among others (Clapp et al., 2001; Huo et al., 2008). Such analyses are relatively rapid and can be performed on unperturbed natural waters from field sites or for a time series of effluent solutions derived from reactive transport experiments.

This study investigated competitive sorption processes during the sequential infusion of two distinct DOM sources (from grassland vegetation and mixed conifer forest) separated in time by a drying event to model a field scenario of two distinct hydrologic events that introduced likewise distinct DOM sources into the soil column (e.g., via vertical and lateral hydrologic flow paths). Specifically, we hypothesized that DOM from the second source (mixed conifer forest) can effectively displace mineral-sorbed OM retrained following the first infusion event (grassland), revealing a kinetically mobile pool of SOM. Further, we postulated that this exchange process would occur despite the greater aromaticity and apparent humification of the OM from the grassland source.

The specific objectives of this study were, therefore, (i) to investigate the role of Al- and Fe-(oxy)hydroxide coatings in the stabilization of DOM derived from grassland and mixed conifer organic horizons during progressive surface loading via saturated column experiments, (ii) to use fluorescence spectroscopy as a tool to monitor effluent DOM solutions and thereby infer sorption–desorption and competitive fractionation during reactive transport, and (iii) to present empirical evidence to support or refute the hypothetical zonal model of organo-mineral interactions.

Materials and Methods

Sample Collection and Dissolved Organic Matter Extraction

Organic (O) horizons (the uppermost 5 cm) were collected in September 2010 from grassland (G) and mixed conifer forest (F) stands established in adjacent locations within an instrumented zero-order basin (a small upland basin with no channel that drains sporadically into a first-order channeled basin) of the La Jara catchment, Valles Caldera National Preserve (Jemez Springs, NM). The study site was chosen because it represents montane forested catchments common in the western United States. Samples were sealed in

zip-lock bags and stored at 4°C. Upon arrival at the Environmental Biogeochemistry Laboratory at the University of Arizona, field-moist samples were sieved (<2 mm), homogenized, and stored at 4°C.

One hundred grams of field-moist material and 500 g of ultrapure (Barnstead) water (giving solid/solution mass ratios of 1:9 for the grassland and 1:13 for the forest) were added to a 1-L bottle that was capped and placed on a reciprocal shaker at 100 rpm for 1 h. Solutions were transferred to 250-mL polypropylene copolymer (PPCO) centrifuge bottles (for which dissolved organic C [DOC] release during the transfer time was measured to be negligible) and centrifuged at 10,000 rpm (15,182 relative centrifugal force [RCF]) for 30 min to sediment the solids. The supernatant solution was transferred into 50-mL PPCO centrifuge tubes and centrifuged again at 18,500 rpm (44,003 RCF) for 20 min to remove polymerized material and the clay fraction. Supernatants were filtered through a precombusted and cleaned 0.7-μm glass fiber filter and 0.01 mol L^{-1} NaN_3 was added to avoid subsequent microbial alteration. The DOM solutions were stored at 4°C for no more than 12 h before use in experiments.

Chemical Characterization of Dissolved Organic Matter Extracts

Several analytical methods were used to assess the chemical character of the extracted DOM solutions (Table 1). The pH was analyzed by electrode (VWR sympHony Model SP80PC), whereas nonpurgeable (total) organic C (TOC) was determined using high temperature oxidation followed by infrared detection of CO_2 (Shimadzu TOC-VCSH, Columbia, MD). DOM elemental composition was determined by inductively coupled plasma mass spectrometry (ICP–MS) (PerkinElmer DRC II, Shelton, CT). The UV-Vis absorbance was determined at 280 nm in order to be able to calculate molar absorptivity values (Shimadzu 2501PC UV-Vis spectrometer). Excitation–emission matrix fluorescence spectra were obtained with the FluoroMax-4 from HORIBA Jobin Yvon equipped with a 150-W Xe-arc lamp source. The EEM spectrum was acquired with excitation (Ex) from 200 to 450 nm and emission (Em) from 250 to 650 nm in 5-nm increments. Spectra were collected with Ex and Em slits at 5- and 2-nm band widths, respectively, and an integration time of 0.1 s. MATLAB R2010a was used to produce EEM contour plots. The fluorescence intensity of 0.003 mol L^{-1} NaN_3 (after threefold dilution, which corresponds to the dilution applied to effluent samples) showed fluorescence EEMs indistinguishable from nanopure water, indicating that NaN_3 had no detectable effect on the spectroscopic results.

Table 1. Chemical properties of the unreacted (extracted before column irrigation) grassland dissolved organic matter (G-DOM) and forest DOM (F-DOM) obtained from O horizons collected from the zero-order basin study site. The chemical parameters were determined after dilution and before use in the reactive transport.

Parameter	G-DOM	F-DOM
Total organic C, mg L^{-1}	40.8 ± 1.2	43.2 ± 0.2
pH	7.95 ± 0.05	8.00 ± 0.03
ε_{280}†, L mol^{-1} cm^{-1}	710 ± 10	478 ± 4
HIX‡	17.8	8.4
Ionic strength§, mol L^{-1}	1.4×10^{-3}	2.3×10^{-3}
F, mg L^{-1}	0.027	0.049
Cl, mg L^{-1}	3.44	2.07
NO_3, mg L^{-1}	6.97	32.82
SO_4, mg L^{-1}	1.74	0.65
PO_4, mg L^{-1}	2.73	4.90
Si, mg L^{-1}	7.72	8.37
Al, mg L^{-1}	0.77	0.66
Fe, mg L^{-1}	0.40	0.35
Na, mg L^{-1}	0.66	1.70
Mg, mg L^{-1}	1.12	1.96
K, mg L^{-1}	12.67	15.64
Ca, mg L^{-1}	15.66	26.49

† ε_{280} was calculated as UV absorption at 280 nm normalized to the molar dissolved organic C concentrations and cuvette path length.
‡ Humification index = $(\sum I_{Em}\ 435 \rightarrow 480)/(\sum I_{Em}\ 300 \rightarrow 345)$, where I_{Em} is the fluorescence intensity.
§ Calculated by MinteqA2.

Sorbent Preparation

Quartz Sand Coating Procedure

Quartz sand (ThermoFisher Scientific) was cleaned in five steps to ensure a pristine material (to remove any impurity) before use in the experiments. Two hundred grams of sand was added to 1.0 kg of solution in a sealed bottle on a reciprocating shaker (100 rpm). Between each step, the wash solutions were decanted, followed by a thorough rinse with ultrapure water until the solution was clear. The washing solutions and reaction time used for each step were (i) HNO_3 (1.6 mol L^{-1}, 2 h), (ii) NaOH (0.5 mol L^{-1}, 2 h), (iii) HCl (0.1 mol L^{-1}, 24 h), (iv) HCl (pH 5, 24 h), and (v) NaOH (0.5 mol L^{-1}, 2 h). After five subsequent rinses with ultrapure water, the sand was spread out to dry at 105°C for 24 h before being stored in an acid-washed container.

The procedure for coating the quartz sand (particle size of 211 ± 1.4 μm) with Al and Fe oxides was based on prior work (Bolster et al., 2001; Park and Kim, 2010). For the Fe-hydroxide-coated quartz sand, 5.5 g of $FeCl_3 \cdot 6H_2O$ was dissolved in 100 mL of ultrapure water. The solution was transferred to a round-bottom boiling flask and the pH adjusted to 9.0 with 6 mol L^{-1} NaOH. Quartz sand (200 g) was added to the solution and swirled to mix. The pH dropped to about 7 but was then readjusted to 9.0, the suspension was swirled, and the pH was checked again. Once the pH stabilized, the flask was placed onto a rotary evaporator at 80 rpm, preheated to 90°C, and flushed with a blanket of N_2. The pH was checked at 5-min intervals and adjusted with dropwise additions of 1 mol L^{-1} NaOH to maintain a pH of ~9, then returned to the evaporator. Heating continued for 90 min. The coated sand slurry was transferred to a Pyrex baking dish, rinsing the flask with

a small amount of water to aid transfer, and then dried at 150°C for 6 h, rinsed with ultrapure water, then dried again under the same conditions (rinse–dry–rinse–dry).

For Al-hydroxide-coated quartz sand, the general procedure outlined above was followed but using $AlCl_3 \cdot 6H_2O$ (4.4 g) dissolved in 100 mL of ultrapure water. The specific surface areas of the quartz sand (Qtz), Al-hydroxide-coated quartz sand (Al-Qtz), and Fe-hydroxide-coated quartz sand (Fe-Qtz) were 0.0290 ± 0.0006, 1.28 ± 0.01, and 1.31 ± 0.01 $m^2\ g^{-1}$, respectively, based on BET analysis of N_2 adsorption data (Table 2). The (oxy)hydroxide surface coatings were loaded with 1.30 ± 0.02 and 2.97 ± 0.46 $g\ kg^{-1}$ of total solid-phase mass for Al and Fe, respectively, as determined after microwave digestion with 16 mol L^{-1} HNO_3, which equates to similar molar loadings, i.e., ~0.05 mol Al or Fe kg^{-1} sorbent, respectively. The mineralogical compositions of the (oxy)hydroxide coatings have been shown previously to comprise microcrystalline gibbsite and hydrous ferric oxide (ferrihydrite), respectively (Bolster et al., 2001; Park and Kim, 2010).

Column Packing and Setup

Baked glass chromatography columns were packed with Qtz, Al-Qtz, and Fe-Qtz. A borosilicate fritted disk and glass wool with medium porosity were placed at the inlet and outlet of the column. The inner diameter and length of the columns were 1.2 and 12 cm, respectively. The average bulk density, particle density, and porosity of the columns were 1.22 ± 0.01 g cm^{-3}, 2.8 ± 0.1 g cm^{-3}, and 0.57 ± 0.02, respectively. A peristaltic pump (Masterflex L/S) was used to drive a constant upward column throughflow of 0.04 mL min^{-1}, which translates to a Darcy flux of 0.06 cm min^{-1}, slow enough to enable a high fluid–mineral interaction time. The upward solution flux was used to diminish preferential flow and ensure uniform water saturation.

Dissolved Organic Matter Reactive Transport Column Experiments

Each Qtz, Al-Qtz, or Fe-Qtz column experiment was run in duplicate and comprised two experimental phases. The first phase involved initial irrigation of fresh mineral media with grassland (G) DOM. The G-DOM solution was diluted with ultrapure water to give a DOC concentration of 40 mg L^{-1} and pH 7.95 to achieve similar DOC concentrations as those measured in pore waters at the study site, which ranged from 10 to 60 mg L^{-1} during the snowmelt season of WY 2011 (Vázquez-Ortega, 2013). During this phase, ~60 pore volumes (PVs) were eluted. The effluent solution was collected every 150 min using a fraction collector (Foxy 200, Teledyne Isco Inc.) for a total volume of 6 mL (equivalent to 1 PV) at each increment. At the end of Phase 1, fluid flow was stopped. The residual solution was extracted by air displacement and included in the last effluent sample, and then the columns were dried in a vacuum chamber (67-kPa air pressure) for 7 d at room temperature (desiccant material was installed within the chamber to absorb water vapor). After the drying period, columns were reinstalled at the pump (Phase 2). This phase consisted of re-irrigation of the OM-coated mineral surfaces with a mixed conifer forest (F) DOM solution with a DOC concentration of 43 mg L^{-1} and pH 8 to model the OM–sorbate exchange that might occur during infusion of DOM from adjacent forest vegetation into grassland soils. This solution was applied at the same flow rate as Phase 1 (0.04 mL min^{-1}) for collection of ~60 PV.

Table 2. Specific surface area (SSA) for the unreacted and reacted oxides and adsorbed organic C (OC) onto the surface of Al-hydroxide-coated quartz sand (Al-Qtz) and Fe-hydroxide-coated quartz sand (Fe-Qtz) after reactive transport.

Mineral	Unreacted SSA†	Reacted SSA‡	Mass-basis adsorbed OC	SSA-basis adsorbed OC
	$m^2\ g^{-1}$		mg C kg^{-1}	mg C m^{-2}
Al-Qtz	1.28 ± 0.01	0.78 ± 0.03	244 ± 3	0.19 ± 0.002
Fe-Qtz	1.31 ± 0.01	1.04 ± 0.07	190 ± 13	0.15 ± 0.01

† Pristine Al- and Fe-(oxy)hydroxide surfaces.
‡ End of Phase 2.

Effluent solutions from PVs 1, 2, 3, 4, 5, 10, 20, 30, and 60 were analyzed from each replicated column to obtain data on pH, Al, Fe, Si, TOC, molar absorptivity, and fluorescence excitation–emission using the methods described above. The UV-Vis and fluorescence spectra were measured on eluted solutions after a threefold dilution was obtained to minimize the inner filter effect (Hudson et al., 2007; Baker et al., 2008). (The inner filter effect is defined as absorption and re-emission at a longer wavelength of incident radiation by the surrounding molecules including the solvent [Hudson et al., 2007]). The humification index (HIX) was calculated from EEMs for all DOM breakthrough curves. The HIX, derived from intensity calculations pertaining to individual fluorescence excitation–emission spectra, has been used to determine the degree of DOM recalcitrance as a result of the degree of molecular complexity and condensation (Zsolnay et al., 1999; Kalbitz et al., 2003). The HIX is defined as sum of the fluorescence intensity (I_{Em}) in the 435- to 480-nm region normalized by that of the 300- to 345-nm region for a specific excitation wavelength of 255 nm:

$$\mathrm{HIX} = \frac{\sum\left(I_{\mathrm{Em}}\,435 \rightarrow 480\right)}{\sum\left(I_{\mathrm{Em}}\,300 \rightarrow 345\right)} \qquad [1]$$

To examine the classes of fluorophores undergoing preferential retention and exchange, fluorescence regional integration (FRI) was calculated for all treatments (Chen et al., 2003). This quantitative technique was developed to integrate the volume within selected regions beneath an EEM surface. The volume (ϕ_i) beneath the ith region of the EEM is calculated as

$$\phi_i = \sum_{\mathrm{ex}} \sum_{\mathrm{em}} I\left(\lambda_{\mathrm{ex}} \lambda_{\mathrm{em}}\right) \Delta_{\mathrm{ex}} \Delta_{\mathrm{em}} \qquad [2]$$

where Δ_{ex} and Δ_{em} are the excitation and emission wavelength intervals, respectively, (both 5 nm) and $I\left(\lambda_{ex}\lambda_{em}\right)$ is the

fluorescence intensity at each excitation–emission wavelength pair. The volume ϕ_i beneath each ith region was normalized to the volume of the same region in the unreacted DOM EEM spectrum (ϕ_0). Values near 1 indicate that the fluorescence intensity of the effluent solution is similar to that of the influent, implying no preferential adsorption of compounds fluorescing in that region. Values <1 indicate preferential adsorption and values >1 indicate preferential desorption and mobilization.

Significant differences among treatments were determined after calculating the 95% confidence interval. Data points shown in all figures represent the mean of duplicate samples extracted at a given pore volume, with error bars representing the 95% confidence interval, with statistically significant ($\alpha = 0.05$ level) differences being represented by those cases where error bars do not overlap.

Results

Dissolved Organic Matter Sorption during Reactive Transport through Pristine Media (Phase 1)

During Phase 1, equivalent grassland DOM solutions were infiltrated into two replicated columns of (i) Qtz, (ii) Al-Qtz, and (iii) Fe-Qtz, enabling an evaluation of the effects of mineral surface chemistry on DOM sorption and fractionation. Effluent pore volumes were analyzed for pH, DOC, UV-Vis absorption, and fluorescence emission. Treatment effects on reactive transport of DOM are apparent from the data comparing effluent solution pH, DOC, molar absorptivity, and HIX (Fig. 1) with values for the influent solution (blue bands represent the influent chemistry inclusive of 95% confidence intervals). For the Qtz treatment, pH values were similar to those of the influent solution, whereas for the Al-Qtz treatment, pH values of the first PVs were lower than the influent, a maximum pH was reached at 10 PVs, and then a subsequent decrease was observed with increasing solution flux through the remainder of Phase 1. The Qtz treatment showed slightly higher DOC concentrations than the influent solution, consistent with small amounts released during the control experiment (not shown), presumably from reagents used in sample preparation. In comparison to the Qtz treatment, Al- and Fe-oxide surface coatings significantly diminished effluent solution concentrations of DOC for the initial 30 PVs of Phase 1. Integrating the mass loss of DOC during the first 30 PVs and normalizing that to the total mass of mineral media present in the columns gives sorbed concentrations of organic C at 30 PVs of 244 ± 3 and 190 ± 13 mg kg^{-1} for Al-Qtz and Fe-Qtz, respectively. Importantly, net dissolution of the Al- and Fe-(oxy)hydroxide coatings was apparently minimal during the course of the experiment (both Phase 1 and Phase 2) because effluent solution concentrations of Al, Fe, and Si were similar to those in the influent solution (Supplemental Fig. S1). Total Si, Al, and Fe concentrations in influent G-DOM were 7.72, 1.98, and 0.80 mg L^{-1} respectively, whereas for F-DOM, corresponding concentrations were 8.4, 1.9, and 0.84 mg L^{-1}. Concentrations of Al and Fe in the effluent solutions remained roughly equivalent to the influent concentrations throughout the course of the experiment, whereas sorptive release of Si was observed in the Qtz case and its sorptive retention was observed in the Al-Qtz and Fe-Qtz cases (Supplemental Fig. S1).

Molar absorptivity (ε) values (Fig. 1C) were calculated from UV absorbance at 280 nm normalized to the molar DOC concentrations and cuvette path length for influent (solid blue line) and effluent (data points) solutions. Molar absorptivity has been shown to correlate positively with DOM aromaticity as measured by ^{13}C nuclear magnetic resonance spectroscopy (Chin et al., 1994) and hence here reflects the fractionation of aromatic DOM moieties relative to bulk constituents on transport through the pristine mineral assemblages. Molar absorptivity values for the Qtz treatment were comparable to

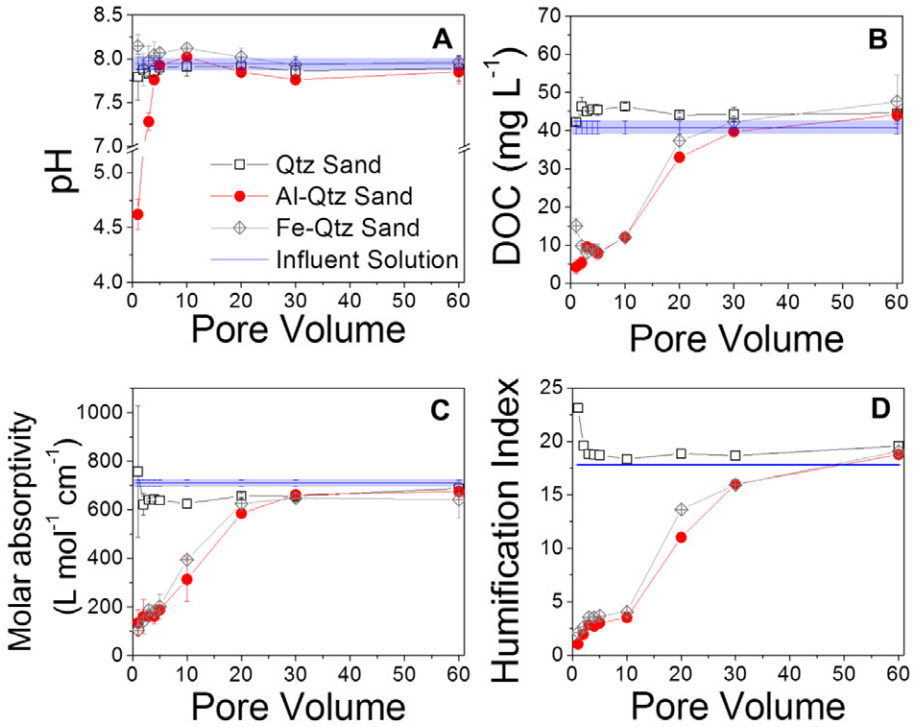

Fig. 1. The (A) pH, (B) dissolved organic C (DOC), (C) molar absorptivity, and (D) humification index (HIX, Eq. [1]) values for quartz sand (Qtz), Al-hydroxide-coated quartz sand (Al-Qtz), and Fe-hydroxide-coated quartz sand (Fe-Qtz) during the initial irrigation of fresh mineral media with grassland dissolved organic matter (Phase 1). Solid blue lines represent the average value for pH, DOC, molar absorptivity, or HIX of the influent solution. Shaded blue bar represents the y error (95% confidence limit) of the influent solution values. Error bars for all treatments represent 95% confidence limits.

the influent value, indicating little fractionation, whereas ε values were diminished significantly during the first 30 PVs for the Al-Qtz and Fe-Qtz treatments, indicating preferential (oxy)hydroxide sorption of aromatic constituents. The ε values during Phase 1 exhibited the following trend: Al-Qtz ≤ Fe-Qtz << Qtz.

Humification index values for effluent solutions from the Qtz treatment were (after 1 PV) similar to that of the influent solution (G-DOM HIX = 17.6, Fig. 1D). For both Al-Qtz and Fe-Qtz treatments, HIX values decreased during the first 30 PVs of Phase 1 with respect to the influent solution value. For these treatments, HIX values increased with time, eventually reaching values similar to the influent solution. The lowest HIX values for Al-Qtz and Fe-Qtz treatments for early PVs were 1.04 and 2.13, respectively—similar to values reported by Kalbitz et al. (2003) to present high biodegradation rates and therefore indicative of more recalcitrant DOM stabilization at pristine (oxy)hydroxide surfaces.

Chen et al. (2003) separated synchronous EEMs (i.e., the excitation–emission fluorescence "surface" as depicted, e.g., in Fig. 2 for G- and F-DOM sources) into five operational regions that have been adopted to quantify DOM molecular variation in the present study: I (aromatic protein I), II (aromatic protein II), III (fulvic-acid-like), IV (soluble microbial byproduct-like), and V (humic-acid-like). The EEMs for unreacted G- and F-DOM solutions, before column application, are shown in Fig. 2. The EEM spectrum for the G-DOM solution shows two principal peaks (Ex: 210 nm, Em: 450 nm and Ex: 260 nm, Em: 460 nm) in Regions III and V, respectively (Fig. 2A).

To probe the EEM spectral "fingerprint" of the DOM that was preferentially retarded during transport as sorbate organic matter (i.e., G-SOM) in each treatment, the EEM spectra of effluent solution samples collected as a function of PV were subtracted from the unreacted G-DOM EEM (Fig. 2) to provide spectroscopic data on fluorophores removed from (and added to) solution. In this case, higher intensities (dark colors) are indicative of G-SOM fluorescent constituents preferentially adsorbed and hence resulting in a net loss of fluorescence in the effluent relative to the influent solution (Fig. 3). In contrast, in accordance with the scale bar shown on the right side of the panels, light colors (pale beige and white) are indicative of DOM desorbed or mobilized from the organo-mineral interface (i.e., net accumulation of fluorescence in the effluent relative to the influent solution) (Fig. 3). For Qtz, all EEM spectral "fingerprints" showed little or no fluorescence emission in the fulvic- and humic-acid-like regions, indicating little or no adsorption to the quartz surface by compounds fluorescent in these regions. For both Al-Qtz and Fe-Qtz, PVs 1 to 5 and 10 showed evidence of high depletions of fluorescence emission in Regions III and V, suggesting preferential adsorption of fulvic- and humic-acid-like (i.e., carboxylic and phenolic) materials onto the Al- or Fe-oxide-coated quartz sand surfaces. By PV 20, the difference between influent and effluent EEMs was still present for these two treatments. Importantly, by 60 PV, desorption was observed, consistent with the DOC results showing effluent solutions exceeding influent concentrations (Fig. 1B).

Fluorescence regional integration ratios revealed that during Phase 1 (Fig. 4, left side), adsorption to the Qtz surface resulted in only modest fractionation, with an apparent preference for sorption of aromatic protein-like fluorophores (Regions I and II, Fig. 4A). Conversely, a distinct separation of fluorophore classes was observed for both the Al-Qtz and Fe-Qtz cases (Fig. 4B and 4C). For the Al-Qtz treatment, FRI ratios indicated that fulvic-acid-like, soluble microbial byproduct-like, and humic-acid-like compounds were preferentially adsorbed to the pristine mineral surface, particularly during early PVs, with preferential adsorption following a trend of V > IV > III > II > I (Fig. 4B). Similarly, during the early PVs of the Fe-Qtz treatment in Phase 1, FRI ratios indicated that compounds in Regions II, III, IV, and V were preferentially adsorbed onto the Fe-hydroxide-coated quartz sand surface. The adsorption trend was as follows: V > IV ≥ III > II > I (Fig. 4C).

By directly comparing HIX and molar absorptivity values, it appears that constituents with lower molar mass and aromaticity were preferentially eluted during the reactive transport for the Al-Qtz treatment and that toward the end of the experiment, effluent constituents resembled those of the influent solution. All data points for the Qtz treatment were clustered next to the influent solution value.

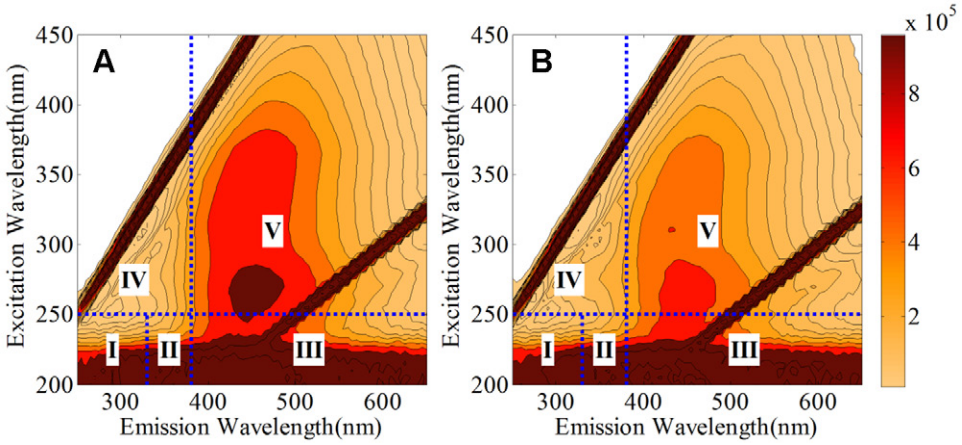

Fig. 2. Excitation–emission matrix spectra for unreacted (A) grassland dissolved organic matter (DOM) and (B) mixed conifer forest DOM solutions. Regions I to V correspond to (Chen et al., 2003): I, aromatic protein I; II, aromatic protein II; III, fulvic-acid-like; IV, soluble microbial byproduct-like; and V, humic-acid-like DOM components.

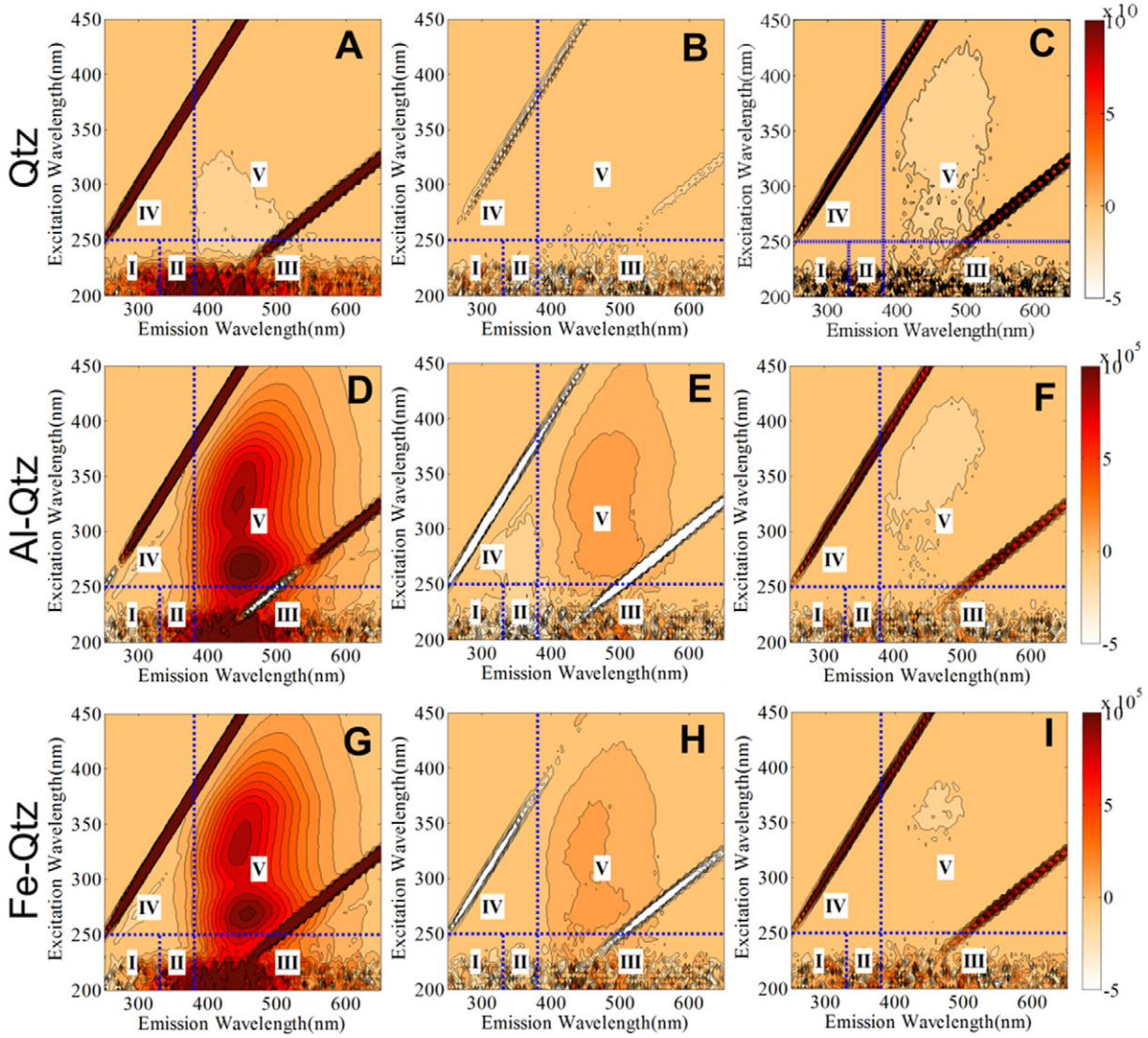

Fig. 3. Excitation–emission matrix (EEM) spectral "fingerprint" of grassland sorbate organic matter (G-SOM) (obtained by subtracting effluent solution from influent grassland dissolved organic matter [G-DOM] solution EEM) for the quartz sand (Qtz), Al-hydroxide-coated quartz sand (Al-Qtz), and Fe-hydroxide-coated quartz sand (Fe-Qtz) treatments during the initial irrigation of fresh mineral media with G-DOM (Phase 1). Each spectrum corresponds to: (A) Qtz, pore volume (PV) 1, (B) Qtz, PV 20, (C) Qtz, PV 60, (D) Al-Qtz, PV 1, (E) Al-Qtz, PV 20, (F) Al-Qtz, PV 60, (G) Fe-Qtz, PV 1, (H) Fe-Qtz, PV 20, and (I) Fe-Qtz, PV 60. Positive values (dark colors) are indicative of G-SOM fluorescent constituents preferentially adsorbed, and negative values (pale beige and white color) are indicative of DOM desorbed or mobilized from the organo–mineral interface. Regions I to V correspond to (Chen et al., 2003): I, aromatic protein I; II, aromatic protein II; III, fulvic-acid-like; IV, soluble microbial byproduct-like; and V, humic-acid-like DOM components.

Dissolved Organic Matter Exchange during Reactive Transport through Organic Matter–Mineral Media (Phase 2)

At the initiation of Phase 2, as a result of the earlier infusion of G-DOM, the Al-Qtz and Fe-Qtz columns contained 244 ± 3 and 190 ± 13 mg kg^{-1} (C basis) of G-SOM (calculated from the C mass differences in influent and effluent solutions). Columns were reinstalled at the pump and infused with F-DOM solution from the mixed conifer forest floor extractions. Relative to the input F-DOM solution (shown in blue bands), all treatments exhibited slightly lower pH values in the effluent relative to influent solutions during 1 to 2 PVs but rapidly converged to within 0.2 pH units of influent values thereafter (Fig. 5A). In stark contrast to Phase 1, all Phase 2 treatments released DOC at concentrations in excess of influent concentrations throughout nearly all of the experiment (Fig. 5B). Values of DOC concentrations were particularly elevated during the first 5 PVs and PV 20, indicating mobilization of G-SOM from the organic–mineral interface (Fig. 5B). An inverse relation was observed between pH and DOC concentration, even in the case of PV 20, which shows a pulsed DOC release (Fig. 5A and 5B).

In contrast to Phase 1, molar absorptivity (ε) values in the effluent DOM solutions were close (within 13%) to those of the influent concentrations throughout all of Phase 2, despite some clear and consistent trends in the data (Fig. 5C). However, it is important to note that the ε value for unreacted F-DOM (478 L mol^{-1} cm^{-1}) was much lower than that for G-DOM (710 L mol^{-1} cm^{-1}), consistent

with G-DOM being more aromatic (Sanderman et al., 2008). It is evident that both the Al-Qtz and Fe-Qtz treatments had lower ε values in PV 20 than the influent, consistent with mobilization of DOC being dominated by low-aromaticity compounds. Early PVs from the Qtz system showed an initial release of the high-ε DOM followed by a progressive decrease toward influent ε values, i.e., an initial trend with PVs that is the opposite of the (oxy)hydroxide-coated surfaces. Furthermore, the pulsed DOC release at ~PV 20 that occurred in all columns (Fig. 5B) was evidently comprised of relatively low-ε DOM in all cases (Fig. 5C). In addition to having a lower ε value than the influent G-DOM, the influent F-DOM solution also had a lower HIX value (8.5 relative to 17.6 for G-DOM). Hence, effluent solutions showed consistently high HIX values relative to influent F-DOM during the entire experiment (Fig. 5D), consistent with displacement of higher HIX G-SOM that was preferentially removed from solution during Phase 1 (Fig. 1D).

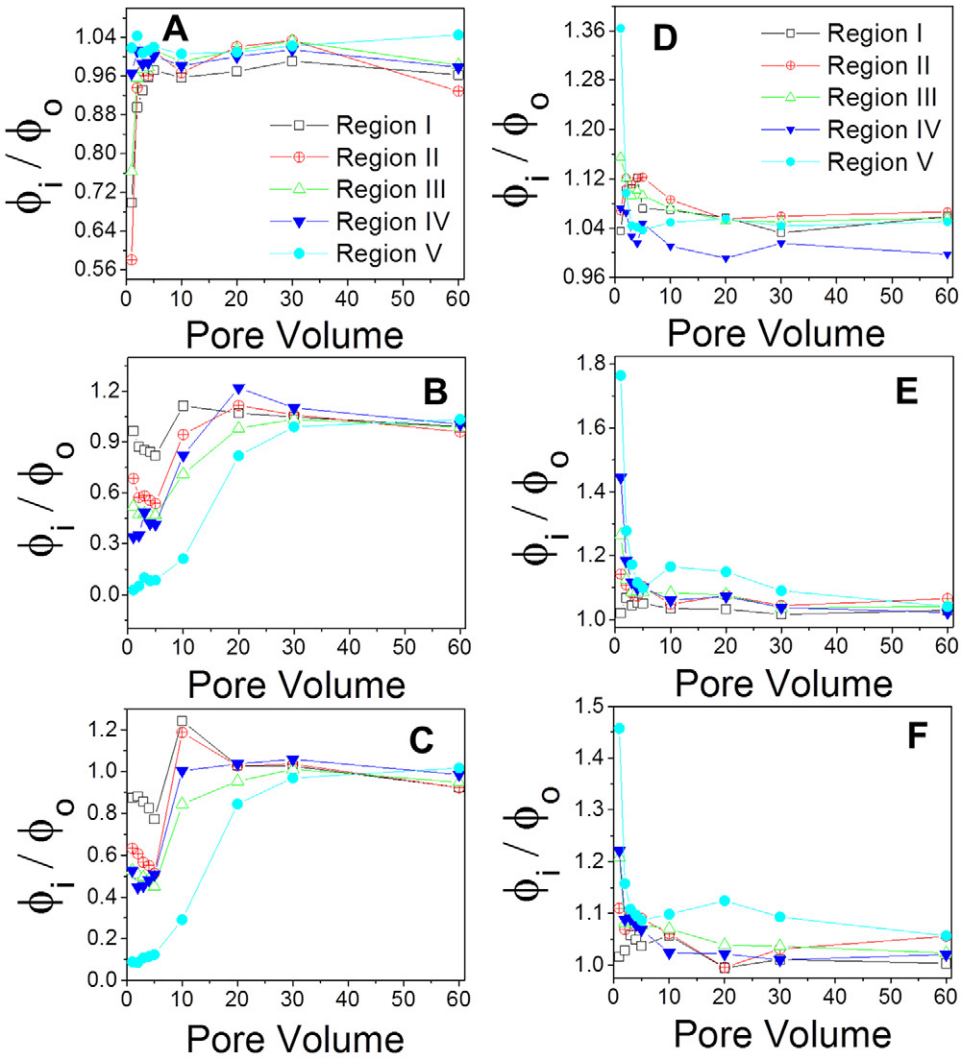

Fig. 4. Fluorescence regional integration (Eq. [2]) of effluent dissolved organic matter (DOM) during transport of grassland DOM through porous media comprising initially pristine mineral surfaces (left column) and mixed conifer forest DOM solution influent to grassland sorbate organic matter coated porous media surfaces (right column): (A,D) quartz sand, (B,E) Al-hydroxide-coated quartz sand, and (C,F) Fe-hydroxide-coated quartz sand. Regions I to V correspond to (Chen et al., 2003): I, aromatic protein I; II, aromatic protein II; III, fulvic-acid-like; IV, soluble microbial byproduct-like; and V, humic-acid-like DOM components.

All treatments showed that the large net G-SOM release occurring throughout the duration of Phase 2 was the result of preferential release of fluorophores associated with Regions V and III of the EEMs (Fig. 6), i.e., preferential desorption of G-SOM constituents characterized by humic-acid-like and fulvic-acid-like fluorescence, respectively (Chen et al., 2003). The greatest mobilization of G-SOM compounds was observed during the first PV for all treatments. During Phase 2, FRI ratios were consistently close to or higher than 1 (Fig. 4, right side). For those constituents exhibiting the greatest preferential adsorption in Phase 1 (Regions III and V), the first PV exhibited the highest FRI ratios, particularly in systems with (oxy)hydroxide coatings.

Discussion

The current study modeled experimentally the infiltration and breakthrough of an initial G-DOM solution—characterized by high HIX and ε values—into pristine porous mineral media (Phase 1) followed by drying and then re-infiltration of a second F-DOM solution with lower HIX and ε values (Phase 2). This order (G-DOM then F-DOM) was selected because it was of interest to assess the extent to which the more aromatic, higher HIX material was displaceable, since DOM of higher aromaticity is known to be preferentially adsorbed to hydroxylated mineral surfaces. This design, applied across three mineralogical treatments (Qtz, Al-Qtz, and Fe-Qtz) permitted the testing of hypotheses related to the impacts of (oxy)hydroxide coatings on retardation of DOM during reactive transport, the impacts of progressive SOM coating on such retardation effects, and the effects of sorbate-coated surfaces on subsequent DOM breakthrough patterns and competitive exchange reactions. The drying step was expected to diminish the likelihood of desorption and exchange of the G-SOM because it removes, to some extent, water molecules that may be interposed between adsorbate molecules and mineral surfaces and between sorbate molecules themselves, thereby promoting the formation of

stronger sorbate–sorbent bonds. Thus, we expect that drying resulted in the formation of stronger DOM–mineral bonds than might have occurred if the drying step had not been included.

Effects of (Oxy)Hydroxide Coatings on Dissolved Organic Matter Transport through Quartz Sand

Surficial (oxy)hydroxide coatings play a major role in regulating the sorption–desorption reactions of DOM. Prior work has shown that oxide coatings strongly alter reaction affinity and molecular mechanisms of sorption of both organic and inorganic solutes (e.g., Benjamin et al., 1996; McMeen and Benjamin, 1997; Korshin et al., 1997; Axe and Trivedi, 2002; Dong et al., 2002; Gupta et al., 2005; Joo et al., 2008; Kaplan Bekaroglu et al., 2010). McMeen and Benjamin (1997) reported high removal of natural organic matter when Fe-(oxy)hydroxide coated sand was present in the system. In the current study, Al- and Fe-(oxy)hydroxide coatings again significantly retarded DOM transport. From the breakthrough curve data (Fig. 1B), we calculated the specific surface area (SSA) normalized DOC sorption values for Al-Qtz and Fe-Qtz media to be 0.19 ± 0.002 and 0.15 ± 0.01 mg C m^{-2}, respectively (Table 2), comparable to prior reports (Gu et al., 1994; Chorover and Amistadi, 2001; Joo et al., 2008). Our results indicate that DOM exhibited a slightly higher affinity for Al-Qtz than for Fe-Qtz treatments, a finding similar to that reported by Banaitis et al. (2006), who equilibrated DOM solutions with pure gibbsite and goethite minerals.

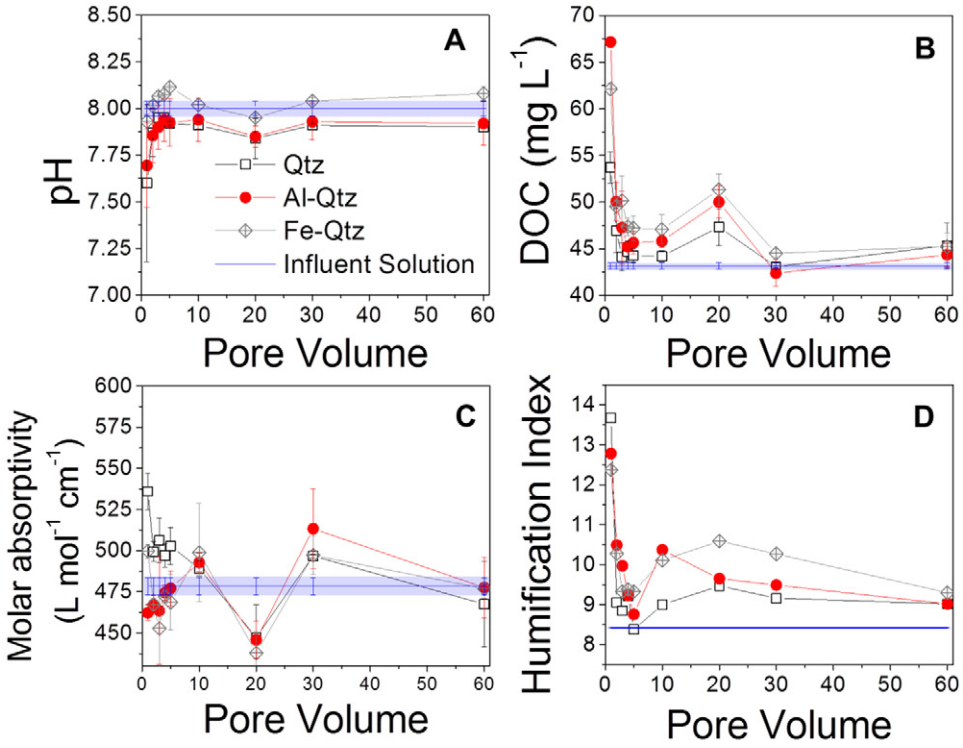

Fig. 5. The (A) pH, (B) dissolved organic C (DOC), (C) molar absorptivity, and (D) humification index (HIX, Eq. [1]) values for quartz sand (Qtz), Al-hydroxide-coated quartz sand (Al-Qtz), and Fe-hydroxide-coated quartz sand (Fe-Qtz) during the re-irrigation of organic-matter-coated mineral surfaces with mixed conifer dissolved organic matter (Phase 2). Solid blue lines represent the average value for pH, DOC, molar absorptivity, or HIX of the influent solution. Shaded blue bar represents the *y* error (95% confidence limit) of the influent solution values. Error bars for all treatments represent 95% confidence limits.

Surface conditioning by both (oxy)hydroxide and SOM coatings were shown in this study to play a major role in subsequent surface reactivity toward DOM and the nature of ensuing fractionation reactions. Specifically, we found that while aromatic (high-ε) and high-HIX moieties (predominantly attributable to lignin phenols) were preferentially adsorbed to pristine (oxy)hydroxide-coated surfaces (G-DOM, Phase 1), introduction of a F-DOM solution of much lower aromaticity and HIX can promote desorption and mobilization of these adsorbate G-DOM species (Phase 2). These findings are in agreement with those of Kaiser and Zech (1998), who examined the sorption of a forest floor DOM and its hydrophilic and hydrophobic fractions to a Bs horizon before and after modifying the surface with DOM and (oxy)hydroxide [amorphous $Al(OH)_3$, ferrihydrite, and goethite] coatings. They found that additions of DOM reduced the sorption of freshly added DOM. Similarly, Weigand and Totsche (1998) also reported high DOM mobilization after the reapplication of DOM solution, attributing the effect to blockage of reactive sorption sites. The blockage of reactive sorption sites in the (oxy)hydroxide coatings used in this study can be tested by comparing the SSA in the unreacted (pristine) vs. reacted minerals (at the end of Phase 2). Initially (before reaction with G-DOM), Al-Qtz and Fe-Qtz exhibited SSA values of 1.28 ± 0.01 and 1.31 ± 0.01 m^2 g^{-1}, respectively. Similar SSA values for Fe- and Al-coated sands have been reported in the literature (Benjamin et al., 1996; Jeong et al., 2007; Lo et al., 1997). At the end of Phase 2 (after reaction with both DOM sources), the SSA of Al-Qtz was reduced to 0.78 ± 0.03 m^2 g^{-1} and that of Fe-Qtz was 1.04 ± 0.07 m^2 g^{-1}, indicating diminished availability of the reactive interface for both sorbent types.

Insights into the implications of the current work for DOM bioavailability were afforded by spectroscopy that showed the time evolution of DOM molecular properties and, by inference, their inherent bioavailability. Compounds with high ε, high HIX, high molar mass, and low carbohydrate content tend to exhibit lower bioavailability (Kalbitz et al., 2003; Hunt and Ohno, 2007). Hence, the fractionation patterns observed in Phase 1 of the current work (pristine mineral surfaces) favored the removal from solution of compounds of (accordingly) greater inherent recalcitrance (from a biodegradation kinetics

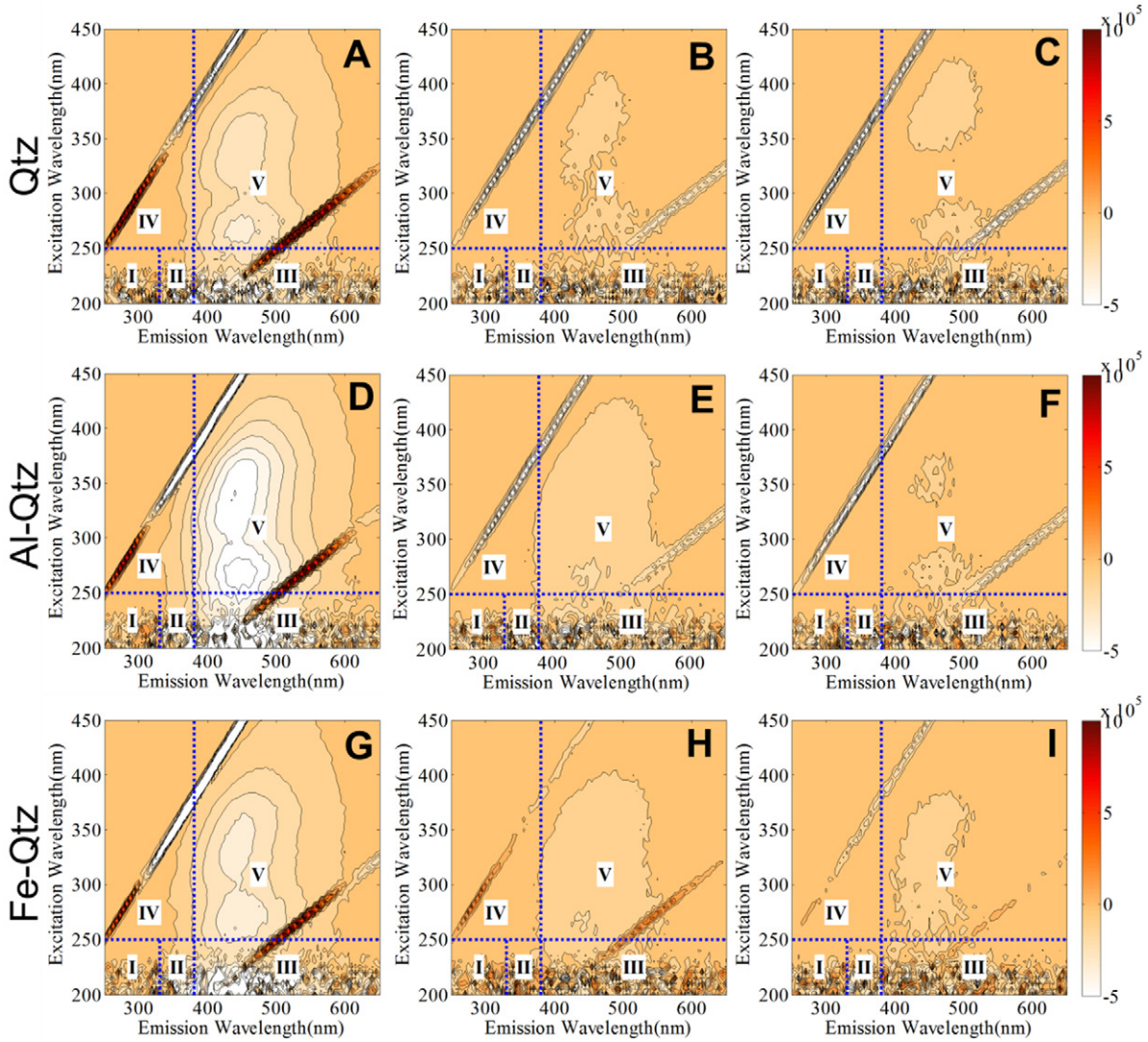

Fig. 6. Excitation–emission matrix spectral "fingerprint" of grassland sorbate organic matter (G-SOM) released from quartz sand (Qtz), Al-hydroxide-coated quartz sand (Al-Qtz), and Fe-hydroxide-coated quartz sand (Fe-Qtz during the re-irrigation of mineral–G-SOM surfaces with mixed conifer forest dissolved organic matter (DOM) solution (Phase 2). Each spectrum corresponds to: (A) Qtz, pore volume (PV) 1, (B) Qtz, PV 20, (C) Qtz, PV 60, (D) Al-Qtz, PV 1, (E) Al-Qtz, PV 20, (F) Al-Qtz, PV 60, (G) Fe-Qtz, PV 1, (H) Fe-Qtz, PV 20, and (I) Fe-Qtz, PV 60. Positive values (dark colors) are indicative of fluorescent constituents preferentially adsorbed and negative values (pale beige and white color) are indicative of DOM desorbed or mobilized from the organo–mineral interface.

standpoint), leaving the more biologically labile pool as mobile to potential receiving groundwater or surface water environments. Indeed, because such sorption reactions probably reduce the accessibility of the otherwise available substrate to microbial and enzymatic degradation (Mikutta et al., 2007, 2011), these partially humified lignin-derived residues would be retained at mineral surfaces with potentially long turnover times and low bioavailability.

Fluorophore-Specific Retardation and Remobilization

The EEM spectral "fingerprints" revealed that fulvic- and humic-acid-like constituents were preferentially retarded by both Al-Qtz and Fe-Qtz minerals during the first PVs of the reactive transport. Likewise, Gu et al. (1996a) showed that organic compounds with a high carboxyl density exhibit a higher competitive adsorption onto the surface of Fe oxide minerals. Several studies have suggested that the principal mechanism by which DOM compounds—probably also involving fulvic- and humic-acid-like constituents—adsorb onto the surface of oxide minerals is ligand exchange–surface complexation (Gu et al., 1994, 1995; Chorover and Amistadi, 2001; Chi and Amy, 2004; Weigand and Totsche 1998; Shen, 1999). Infrared spectroscopy studies provide direct evidence of ligand exchange during surface complexation (Gu et al., 1994; Chorover and Amistadi, 2001). In the current study, a slight increase in pH was observed at PV 5 for the Fe-Qtz treatment (significantly different than the influent solution) (Fig. 1A), suggesting the occurrence of this proton-consuming chemisorptive process:

$$\equiv FeOH_{(s)} + H^{+}_{aq} \rightleftarrows \equiv FeOH^{+}_{2(s)} \quad [3]$$

$$\equiv FeOH^{+}_{2(s)} + R\text{-}COO^{-}_{aq} \rightleftarrows \equiv FeOOC\text{-}R_{(s)} + H_2O_{(l)} \quad [4]$$

In contrast, in Phase 2 a significant displacement and remobilization of G-SOM was observed (Fig. 5B), corresponding primarily to humic-acid-like constituents and to a lesser extent fulvic-acid-like constituents (Fig. 6). That is, during re-irrigation (Phase 2, irrigation with F-DOM), early pore water effluents showed higher DOC concentrations than the influent solution, indicating not only lower sorption of F-DOM onto the mineral surface but also solution-phase remobilization of G-SOM (sorbate). Fluorescence regional integration ratios of effluent DOM during infiltration of F-DOM solution to G-SOM-coated porous media surfaces revealed that Region V exhibited the highest ratios, indicating desorption and mobilization of humic-acid-like compounds from the organic–mineral interface that had been adsorbed during G-DOM irrigation (Fig. 4). The remobilization of high-HIX G-SOM constituents was apparently the result of a continuous displacement of kinetically mobile G-SOM and mixing of influent and sorbate OM constituents that produced a much narrower range of HIX and ε values during the course of Phase 2 (Fig. 7, right side) relative to Phase 1. High-affinity adsorptive species from F-DOM competitively displaced G-SOM molecules that were apparently weakly linked to the mineral surface. Similarly, Gu et al. (1996b) reported that Suwannee River natural organic matter competitively displaced organic acids (phthalic and salicylic) with lower adsorption affinity to Fe-oxide minerals.

The observed desorption of G-SOM during infusion of F-DOM is consistent with—but not unequivocal proof of—the zonal model of OM adsorption at mineral surfaces (Wershaw, 1993; Kleber et al., 2007). From the perspective of this model, molecular mechanisms potentially contributing to desorption of higher HIX G-SOM could involve a combination of organic and inorganic geochemical perturbation effects, including (i) anion exchange in the mineral contact zone, where anionic F-DOM organic and inorganic adsorptives may compete with G-SOM for mineral surface sites, (ii) hydrophobic molecule displacement in the intermediate zone, and (iii) cation or aggregate displacement in the peripheral kinetic zone where inorganic cation exchange reactions in ligand bridging positions may disrupt the supramolecular structure of the G-SOM adsorbate. Each of these may occur during aqueous (bio)geochemical perturbations that subsequently affect the solid–solution exchange of interfacial species, where a diversity of OM binding mechanisms (ligand exchange, cation bridging, van der Waals forces) at mineral surfaces control sorbed OM stabilization (Mikutta et al., 2007).

Given that supramolecular associations of OM may be altered by changes in the background solution chemistry (Sutton and Sposito, 2005), it is important to consider the potential effects of inorganic cations and anions on OM interfacial uptake. As is apparent from inspection of Table 1, the introduction of F-DOM solutions could potentially disrupt the binding interactions in G-SOM, not only because of variation in DOM chemistry but also because of the higher orthophosphate, Ca, and Na concentrations relative to the G-DOM solution. Orthophosphate concentration, which was almost two times higher in F-DOM solution, could induce anion (including ligand) exchange reactions, prompting desorption of aromatic compounds from the organic–mineral interface (Guan et al., 2006; Mikutta et al., 2007). A higher Ca^{2+} concentration in the F-DOM solution could also induce perturbation in the G-SOM aggregates by disrupting cation bridging interactions in the peripheral kinetic zone, e.g., by replacing Na^{+}, K^{+}, and Mg^{2+}. Higher solution ionic strength of F-DOM relative to G-DOM could induce greater aggregation in the former, making F-DOM a more effective competitor for surface sites because of larger apparent supramolecular size (Chorover and Amistadi, 2001).

Geochemical modeling, using a specialized submodel for calculations involving DOM–metal interactions (Susetyo et al., 1991), was conducted to assess the cation species distribution of DOM in unreacted G-DOM and F-DOM solutions (MINTEQA2 for Windows, Version 1.50, Allison Geoscience Consultants, Inc.), with DOC concentration and DOM site density (2.4×10^{-3} mol g^{-1} DOC) as required input parameters. A higher fraction of total Ca was assigned to Ca-DOM species for the F-DOM (0.4) relative to G-DOM (0.3), suggesting that Ca bridging interactions may indeed be more prevalent in the F-DOM solution, a factor potentially contributing to its more effective retention as an adsorbate.

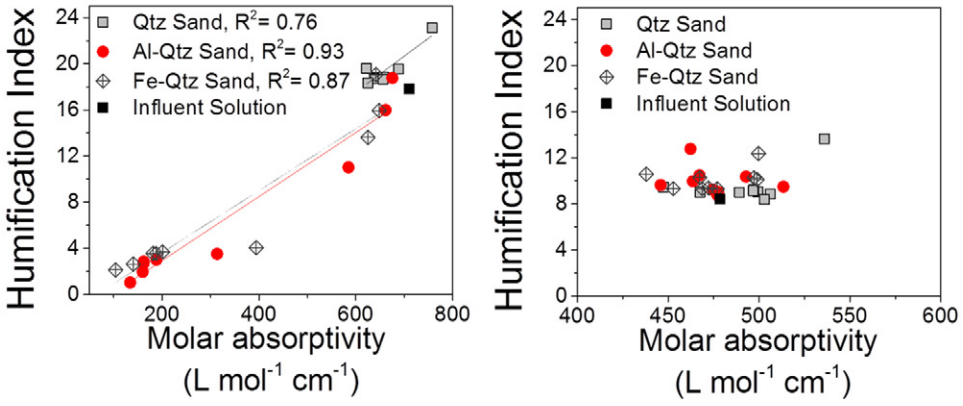

Fig. 7. Scatterplots of humification index from fluorescence excitation–emission spectroscopy vs. molar absorptivity from UV 280-nm absorbance for Phase 1 (left) and Phase 2 (right) of the reactive transport experiments. Note the strong positive correlation between the two variables in Phase 1 during reaction of grassland dissolved organic matter with initially pristine mineral surfaces. In contrast during Phase 2, a much narrower range in values of both variables with no significant correlation is observed.

In summary, the perturbation of the G-SOM aggregates by the introduction of F-DOM solutions comprising a distinct chemical composition could induce desorption of humic-acid-like compounds from the organic–mineral interface. Future experiments that control the details of background inorganic ion chemistry could help to unravel those potential effects.

Conclusions

Flow-through column experiments were conducted to investigate the role of surficial (oxy)hydroxide coatings in DOM fractionation and stabilization during reactive transport. The experiments revealed that pristine Al- and Fe-(oxy)hydroxide coatings on quartz surfaces preferentially sequester aromatic and humified constituents into sorbate form, thereby significantly retarding the transport and, presumably, the bioavailability (not the focus of this study) of these partially degraded lignin phenols. Meanwhile, less aromatic and humified constituents are transported with little retardation. However, progressive conditioning of the (oxy)hydroxide surfaces with SOM resulted in distinctly different transport and retardation behavior in subsequent DOM infiltration events. The infusion of fresh F-DOM into SOM-(oxy)hydroxide-coated quartz sand resulted in displacement of the high-affinity (aromatic and humified) sorbate forms, indicating that SOM constituents can occur in kinetically mobile and exchangeable forms that can be remobilized by perturbation of the pore water chemistry. From the perspective of the zonal model of organo-mineral association, such perturbations can derive from changes in inorganic anion and cation concentrations that influence anion exchange reactions in the mineral contact zone and cation bridging interactions in the peripheral kinetic zone, respectively.

Acknowledgments

This work was supported by National Science Foundation Grants EAR-0724958, EAR-1331408 for the Santa Catalina– Jemez Critical Zone Observatory, and DEB-0543130. We are grateful to three anonymous reviewers and Associate Editor Karsten Kalbitz, whose constructive comments significantly improved the manuscript.

References

Axe, L., and P. Trivedi. 2002. Intraparticle surface diffusion of metal contaminants and their attenuation in microporous amorphous Al, Fe, and Mn oxides. J. Colloid Interface Sci. 247:259–265. doi:10.1006/jcis.2001.8125

Baker, A., E. Tipping, S.A. Thacker, and D. Gondar. 2008. Relating dissolved organic matter fluorescence and functional properties. Chemosphere 73:1765–1772. doi:10.1016/j.chemosphere.2008.09.018

Banaitis, M.R., H. Waldrip-Dail, M.S. Diehl, B.C. Holmes, J.F. Hunt, R.P. Lynch, and T. Ohno. 2006. Investigating sorption-driven dissolved organic matter fractionation by multidimensional fluorescence spectroscopy and PARAFAC. J. Colloid Interface Sci. 304:271–276. doi:10.1016/j.jcis.2006.07.035

Benjamin, M.M., R.S. Sletten, R.P. Bailey, and T. Bennett. 1996. Sorption and filtration of metals using iron-oxide-coated sand. Water Res. 30:2609–2620. doi:10.1016/S0043-1354(96)00161-3

Bieroza, M.Z., J. Bridgeman, and A. Baker. 2010. Fluorescence spectroscopy as a tool for determination of organic matter removal efficiency at water treatment works. CRC Press, Boca Raton, FL.

Bolster, C.H., A.L. Mills, G.M. Hornberger, and J.S. Herman. 2001. Effect of surface coatings, grain size, and ionic strength on the maximum attainable coverage of bacteria on sand surfaces. J. Contam. Hydrol. 50:287–305. doi:10.1016/S0169-7722(01)00106-1

Chen, W., P. Westerhoff, J.A. Leenheer, and K. Booksh. 2003. Fluorescence excitation– emission matrix regional integration to quantify spectra for dissolved organic matter. Environ. Sci. Technol. 37:5701–5710. doi:10.1021/es034354c

Chi, F.-H., and G.L. Amy. 2004. Kinetic study on the sorption of dissolved natural organic matter onto different aquifer materials: The effects of hydrophobicity and functional groups. J. Colloid Interface Sci. 274:380–391. doi:10.1016/j.jcis.2003.12.049

Chin, Y.-P., G. Aiken, and E. O'Loughlin. 1994. Molecular-weight, polydispersity, and spectroscopic properties of aquatic humic substances. Environ. Sci. Technol. 28:1853–1858. doi:10.1021/es00060a015

Chorover, J., and M.K. Amistadi. 2001. Reaction of forest floor organic matter at goethite, birnessite and smectite surfaces. Geochim. Cosmochim. Acta 65:95–109. doi:10.1016/S0016-7037(00)00511-1

Clapp, C.E., M.H.B. Hayes, N. Senesi, P.R. Bloom, and P.M. Jardine, editors. 2001. Humic substances and chemical contaminants. SSSA, Madison, WI.

Coston, J.A., C.C. Fuller, and J.A. Dacis. 1995. Pb^{2+} and Zn^{2+} adsorption by a natural aluminum-bearing and iron-bearing surface coating on an aquifer sand. Geochim. Cosmochim. Acta 59:3535–3547. doi:10.1016/0016-7037(95)00231-N

Dong, H., T.C. Onstott, C.-H. Ko, A.D. Hollingsworth, D.G. Brown, and B.J. Mailloux. 2002. Theoretical prediction of collision efficiency between adhesion-deficient bacteria and sediment grain surface. Colloids Surf. B 24:229–245. doi:10.1016/S0927-7765(01)00243-0

Eusterhues, K., C. Rumpel, M. Kleber, and I. Kögel-Knabner. 2003. Stabilisation of soil organic matter by interactions with minerals as revealed by mineral dissolution and oxidative degradation. Org. Geochem. 34:1591–1600. doi:10.1016/j.orggeochem.2003.08.007

Eusterhues, K., C. Rumpel, and I. Kögel-Knabner. 2005. Organo-mineral associations in sandy acid forest soils: Importance of specific surface area, iron oxides and micropores. Eur. J. Soil Sci. 56:753–763.

Goh, K.M. 2004. Carbon sequestration and stabilization in soils: Implications for soil productivity and climate change. Soil Sci. Plant Nutr. 50:467–476. doi:10.1080/00380768.2004.10408502

Greenland, D.J. 1971. Interactions between humic and fulvic acids and clays. Soil Sci. 111:34–41. doi:10.1097/00010694-197101000-00004

Gu, B., T.L. Mehlhorn, L. Liang, and J.F. McCarthy. 1996a. Competitive adsorption, displacement, and transport of organic matter on iron oxide: I. Competitive adsorption. Geochim. Cosmochim. Acta 60:1943–1950. doi:10.1016/0016-7037(96)00059-2

Gu, B., T.L. Mehlhorn, L. Liang, and J.F. McCarthy. 1996b. Competitive adsorption, displacement, and transport of organic matter on iron oxide: II. Displacement and transport. Geochim. Cosmochim. Acta 60:2977–2992. doi:10.1016/0016-7037(96)00157-3

Gu, B., J. Schmitt, Z. Chen, L. Liang, and J.F. McCarthy. 1994. Adsorption and desorption of natural organic matter on iron oxide: Mechanisms and models. Environ. Sci. Technol. 28:38–46. doi:10.1021/es00050a007

Gu, B., J. Schmitt, Z. Chen, L. Liang, and J.F. McCarthy. 1995. Adsorption and desorption of different organic matter fractions on iron oxide. Geochim. Cosmochim. Acta 59:219–229. doi:10.1016/0016-7037(94)00282-Q

Guan, X.-H., C. Shang, and G.-H. Chen. 2006. Competitive adsorption of organic matter with phosphate on aluminum hydroxide. J. Colloid Interface Sci. 296:51–58. doi:10.1016/j.jcis.2005.08.050

Guo, M., and J. Chorover. 2003. Transport and fractionation of dissolved organic matter in soil columns. Soil Sci. 168:108–118. doi:10.1097/00010694-200302000-00005

Guo, M., and J. Chorover. 2006. Leachate migration from spent mushroom substrate through intact and repacked subsurface soil columns. Waste Manage. 26:133–140. doi:10.1016/j.wasman.2004.12.024

Gupta, V.K., V.K. Saini, and N. Jain. 2005. Adsorption of As(III) from aqueous solutions by iron oxide-coated sand. J. Colloid Interface Sci. 288:55–60. doi:10.1016/j.jcis.2005.02.054

Hedman, K., A.S. Grandy, X. Gao, M. Keiluweit, K. Wickings, K. Carpenter, et al. 2013a. Sorptive fractionation of organic matter and formation of organo-hydroxy-aluminum complexes during litter biodegradation in the presence of gibbsite. Geochim. Cosmochim. Acta 121:667–683.

Hedman, K., A. Welty-Bernard, A. Vazquez-Ortega, E. Schwartz, J. Chorover, and C. Rasmussen. 2013b. The influence of goethite and gibbsite on soluble nutrient dynamics and microbial community composition. Biogeochemistry 112:179–195.

Her, N., G. Amy, D. McKnight, J. Sohn, and Y. Yoon. 2003. Characterization of DOM as a function of MW by fluorescence EEM and HPLC-SEC using UVA, DOC, and fluorescence detection. Water Res. 37:4295–4303. doi:10.1016/S0043-1354(03)00317-8

Hernandez-Ruiz, S., L. Abrell, S. Wickramasekara, B. Chefetz, and J. Chorover. 2012. Quantifying PPCP interaction with dissolved organic matter in aqueous solution: Combined use of fluorescence quenching and tandem mass spectrometry. Water Res. 46:943–954. doi:10.1016/j.watres.2011.11.061

Hudson, N., A. Baker, and D. Reynolds. 2007. Fluorescence analysis of dissolved organic matter in natural, waste and polluted waters: A review. River Res. Appl. 23:631–649. doi:10.1002/rra.1005

Hunt, J.F., and T. Ohno. 2007. Characterization of fresh and decomposed dissolved organic matter using excitation–emission matrix fluorescence spectroscopy and multiway analysis. J. Agric. Food Chem. 55:2121–2128. doi:10.1021/jf063336m

Hunt, J.F., T. Ohno, Z. He, C.W. Honeycutt, and D.B. Dail. 2007. Influence of decomposition on chemical properties of plant- and manure-derived dissolved organic matter and sorption to goethite. J. Environ. Qual. 36:135–143. doi:10.2134/jeq2006.0133

Huo, S., B. Xi, H. Yu, L. He, S. Fan, and H. Liu. 2008. Characteristics of dissolved organic matter (DOM) in leachate with different landfill ages. J. Environ. Sci. 20:492–498. doi:10.1016/S1001-0742(08)62085-9

Jeong, Y., M. Fan, S. Singh, C.-L. Chuang, B. Saha, and J.H. van Leeuwen. 2007. Evaluation of iron oxide and aluminum oxide as potential arsenic(V) adsorbents. Chem. Eng. Process. 46:1030–1039. doi:10.1016/j.cep.2007.05.004

Joo, J.C., C.D. Shackelford, and K.F. Reardon. 2008. Association of humic acid with metal (hydr)oxide-coated sands at solid–water interfaces. J. Colloid Interface Sci. 317:424–433. doi:10.1016/j.jcis.2007.09.061

Kaiser, K., and G. Guggenberger. 2000. The role of DOM sorption to mineral surfaces in the preservation of organic matter in soils. Org. Geochem. 31:711–725. doi:10.1016/S0146-6380(00)00046-2

Kaiser, K., G. Guggenberger, L. Haumaier, and W. Zech. 1997. Dissolved organic matter sorption on sub soils and minerals studied by ^{13}C NMR and DRIFT spectroscopy. Eur. J. Soil Sci. 48:301–310. doi:10.1111/j.1365-2389.1997.tb00550.x

Kaiser, K., R. Mikutta, and G. Guggenberger. 2007. Increased stability of organic matter sorbed to ferrihydrite and goethite on aging. Soil Sci. Soc. Am. J. 71:711–719. doi:10.2136/sssaj2006.0189

Kaiser, K., and W. Zech. 1998. Soil dissolved organic matter sorption as influenced by organic and sesquioxide coatings and sorbed sulfate. Soil Sci. Soc. Am. J. 62:129–136. doi:10.2136/sssaj1998.03615995006200010017x

Kalbitz, K., J. Schmerwitz, D. Schwesig, and E. Matzner. 2003. Biodegradation of soil-derived dissolved organic matter as related to its properties. Geoderma 113:273–291. doi:10.1016/S0016-7061(02)00365-8

Kaplan Bekaroglu, S.S., N.O. Yigit, T. Karanfil, and M. Kitis. 2010. The adsorptive removal of disinfection by-product precursors in a high-SUVA water using iron oxide-coated pumice and volcanic slag particles. J. Hazard. Mater. 183:389–394. doi:10.1016/j.jhazmat.2010.07.037

Kleber, M., P. Sollins, and R. Sutton. 2007. A conceptual model of organo–mineral interactions in soils: Self-assembly of organic molecular fragments into zonal structures on mineral surfaces. Biogeochemistry 85:9–24. doi:10.1007/s10533-007-9103-5

Korshin, G.V., M.M. Benjamin, and R.S. Sletten. 1997. Adsorption of natural organic matter (NOM) on iron oxide: Effects on NOM composition and formation of organo-halide compounds during chlorination. Water Res. 31:1643–1650. doi:10.1016/S0043-1354(97)00007-9

Lam, B., and A.J. Simpson. 2008. Direct ^{1}H NMR spectroscopy of dissolved organic matter in natural waters. Analyst 133:263–269. doi:10.1039/b713457f

Lattao, C., J. Birdwell, J.J. Wang, and R.L. Cook. 2008. Studying organic matter molecular assemblage within a whole organic soil by nuclear magnetic resonance. J. Environ. Qual. 37:1501–1509. doi:10.2134/jeq2007.0137

Lo, S.-L, H.-T. Jeng, and C.-H. Lai. 1997. Characteristics and adsorption properties of iron-coated sand. Water Sci. Technol. 35:63–70. doi:10.1016/S0273-1223(97)00115-7

McMeen, C., and M. Benjamin. 1997. NOM removal by slow sand filtration through iron oxide-coated olivine. J. Am. Water Works Assoc. 89:57–71.

Meier, M., K. Namjesnik-Dejanovic, P.A. Maurice, Y.-P. Chin, and G.R. Aiken. 1999. Fractionation of aquatic natural organic matter upon sorption to goethite and kaolinite. Chem. Geol. 157:275–284. doi:10.1016/S0009-2541(99)00006-6

Mikutta, R., C. Mikutta, K. Kalbitz, T. Scheel, K. Kaiser, and R. Jahn. 2007. Biodegradation of forest floor organic matter bound to minerals via different binding mechanisms. Geochim. Cosmochim. Acta 71:2569–2590. doi:10.1016/j.gca.2007.03.002

Mikutta, R., U. Zang, J. Chorover, L. Haumaier, and K. Kalbitz. 2011. Stabilization of extracellular polymeric substances (*Bacillus subtilis*) by adsorption to and coprecipitation with Al forms. Geochim. Cosmochim. Acta 75:3135–3154. doi:10.1016/j.gca.2011.03.006

Mortland, M.M. 1970. Clay–organic complexes and interactions. Adv. Agron. 22:75–117. doi:10.1016/S0065-2113(08)60266-7

Namjesnik-Dejanovic, K., P.A. Maurice, G.R. Aiken, S. Cabaniss, Y.-P. Chin, and M.J. Pullin. 2000. Adsorption and fractionation of a muck fulvic acid on kaolinite and goethite at pH 3.7, 6, and 8. Soil Sci. 165:545–559. doi:10.1097/00010694-200007000-00003

Ohno, T., A. Amirbahman, and R. Bro. 2008. Parallel factor analysis of excitation–emission matrix fluorescence spectra of water soluble soil organic matter as basis for the determination of conditional metal binding parameters. Environ. Sci. Technol. 42:186–192. doi:10.1021/es071855f

Ohno, T., J. Chorover, A. Omoike, and J. Hunt. 2007. Molecular weight and humification index as predictors of adsorption for plant- and manure-derived dissolved organic matter to goethite. Eur. J. Soil Sci. 58:125–132. doi:10.1111/j.1365-2389.2006.00817.x

Park, S.-J., and S.-B. Kim. 2010. Influence of (bi)carbonate on bacterial interaction with quartz and metal oxide-coated surfaces. Colloids Surf. B 76:57–62. doi:10.1016/j.colsurfb.2009.10.010

Perdrial, J.N., J. McIntosh, A. Harpold, P.D. Brooks, X. Zapata-Rios, J. Ray, et al. 2014. Stream water carbon controls in seasonally snow-covered mountain catchments: impact of inter-annual variability of water fluxes, catchment aspect and seasonal processes. Biogeochemistry 118:273–290. doi:10.1007/s10533-013-9929-y

Sanderman, J., J.A. Baldock, and R. Amundson. 2008. Dissolved organic carbon chemistry and dynamics in contrasting forest and grassland soils. Biogeochemistry 89:181–198. doi:10.1007/s10533-008-9211-x

Scheel, T., C. Dörfler, and K. Kalbitz. 2007. Precipitation of dissolved organic matter by aluminum stabilizes carbon in acidic forest soils. Soil Sci. Soc. Am. J. 71:64–74. doi:10.2136/sssaj2006.0111

Shen, Y.-H. 1999. Sorption of natural dissolved organic matter on soil. Chemosphere 38:1505–1515. doi:10.1016/S0045-6535(98)00371-3

Simpson, A.J., M.J. Simpson, and R. Soong. 2012. Nuclear magnetic resonance spectroscopy and its key role in environmental research. Environ. Sci. Technol. 46:11488–11496. doi:10.1021/es302154w

Six, J., R.T. Conant, E.A. Paul, and K. Paustian. 2002. Stabilization mechanisms of soil organic matter: Implications for C-saturation of soils. Plant Soil 241:155–176. doi:10.1023/A:1016125726789

Susetyo, W., L.A. Carreira, L.V. Azarraga, and D.M. Grimm. 1991. Fluorescence techniques for metal–humic interactions. Fresnius J. Anal. Chem. 339:624–635. doi:10.1007/BF00325549

Sutton, R., and G. Sposito. 2005. Molecular structure in soil humic substances: The new view. Environ. Sci. Technol. 39:9009–9015. doi:10.1021/es050778q

Theng, B.K.G. 1979. Formation and properties of clay–polymer complexes. Elsevier, New York.

Vázquez-Ortega, A. 2013. Coupled transport, fractionation and stabilization of dissolved organic matter and rare earth elements in the critical zone. Ph.D. diss. Dep. of Soil, Water and Environ. Sci., Univ. of Arizona, Tucson.

von Lützow, M., I. Kögel-Knabner, K. Ekschmitt, E. Matzner, G. Guggenberger, B. Marschner, and H. Flessa. 2006. Stabilization of organic matter in temperate soils: Mechanisms and their relevance under different soil conditions: A review. Eur. J. Soil Sci. 57:426–445. doi:10.1111/j.1365-2389.2006.00809.x

von Lützow, M., I. Kögel-Knabner, B. Ludwig, E. Matzner, H. Flessa, K. Ekschmitt, et al. 2008. Stabilization mechanisms of organic matter in four temperate soils: Development and application of a conceptual model. J. Plant Nutr. Soil Sci. 171:111–124. doi:10.1002/jpln.200700047

Weigand, H., and K.U. Totsche. 1998. Flow and reactivity effects on dissolved organic matter transport in soil columns. Soil Sci. Soc. Am. J. 62:1268–1274. doi:10.2136/sssaj1998.03615995006200050017x

Wershaw, R. 1993. Model for humus in soils and sediments. Environ. Sci. Technol. 27:814–816. doi:10.1021/es00042a603

Zhou, Q., P.A. Maurice, and S.E. Cabaniss. 2001. Size fractionation upon adsorption of fulvic acid on goethite: Equilibrium and kinetic studies. Geochim. Cosmochim. Acta 65:803–812. doi:10.1016/S0016-7037(00)00536-6

Zsolnay, A., E. Baigar, M. Jimenez, B. Steinweg, and F. Saccomandi. 1999. Differentiating with fluorescence spectroscopy the sources of dissolved organic matter in soils subjected to drying. Chemosphere 38:45–50. doi:10.1016/S0045-6535(98)00166-0